RSC Advances

ROYAL SOCIETY OF CHEMISTRY

www.rsc.org/advances

Fabrication and enhanced visible-light photocatalytic activities of $BiVO_4/Bi_2WO_6$ composites

Yanling Geng*, Peng Zhang, Shaoping Kuang

College of Chemistry and Molecular Engineering, Qingdao University of Science and Technology, Qingdao, 266042, (China)

Abstract

$BiVO_4/Bi_2WO_6$ composite photocatalysts were synthesized by coupling a homogeneous precipitation method with hydrothermal techniques. The as-prepared samples were characterized by X-ray diffraction (XRD), Fourier transform infrared spectrometer (FTIR), scanning electron microscopy (SEM), energy dispersive spectroscopy (EDS), UV-vis diffusion absorption spectra (DRS) and photoluminescence (PL), respectively. The photocatalytic activities were evaluated by the degradation of methyl blue (MB) under visible-light irradiation. The results reveal that $BiVO_4/Bi_2WO_6$ composites exhibit higher photocatalytic activities than either pure Bi_2WO_6 or $BiVO_4$. The $0.3BiVO_4$:$0.7Bi_2WO_6$ sample shows the best photocatalytic performance. The enhancement of photocatalytic activity is attributed to the improvement of light absorption, the excellent adsorbability, the narrow band gap and increasing separation rate of photo-generated charge carriers. The possible photocatalytic mechanism is discussed on the basis of the band structures of $BiVO_4$

and Bi_2WO_6.

Keyword: Bi_2WO_6; $BiVO_4$; photocatalytic activity; visible light

1. Introduction

In the past decades, semiconductor photocatalysts have attracted much attention due to their promising application in the area of solar energy conversion and degradation of environmental pollutants[1-2]. To date, TiO_2 has proven to be the most popular photocatalyst for its high photocatalytic activity, good chemical stability, non-toxicity and low cost[3]. Unfortunately, the excellent photocatalytic performance of TiO_2 has been confined to the ultraviolet light (λ<400 nm) because of the large band gap (3.2 eV), which greatly restrict its practical application[4]. Therefore, it is quite urgent to exploit new photocatalysts with visible-light-driven photocatalytic ability. In the study of semiconductor materials responding to the visible-light, many attempts have been carried out in the last decade. One method to obtain visible-light-driven photocatalysts is to broaden the photo-response of TiO_2 into visible light region, such as metal ion doping[5], nonmetal doping[6], noble metal deposition[7], and semiconductors coupling[8]. In another approach, several researchers have developed novel photocatalysts with intrinsic visible-light-driven photocatalytic ability, for examples $CaIn_2O_4$[9], $InVO_4$[10], $BiVO_4$[11], Bi_2WO_6[12] and bismuth oxyhalides[13][14].

Among various novel photocatalysts, the typical Aurivillius oxide Bi_2WO_6 has

been considered as an excellent visible light photocatalyst used for degradation of organic pollutants and water splitting[15, 16]. However, the photocatalytic activity of the pure Bi_2WO_6 is relatively low owing to its narrow absorption range of visible light (shorter than 450 nm) and rapid recombination of photo-induced electron-hole pairs[17, 18]. To enhance its photocatalytic performance, doping Bi_2WO_6 with TiO_2[19], Fe[20], $BiIO_4$[21], CdSe[22], SiO_2[23] have been taken to inhibit the recombination of photogenerated holes and electrons successfully.

As is known, $BiVO_4$ with a monoclinic scheelite structure shows photocatalytic activity for O_2 evolution and organic pollutants photodegradation under visible light irradiation[24]. What's more, $BiVO_4$ has suitable band edges (E_{CB} = 0.385 eV, E_{VB} = 2.685 eV), matching well with Bi_2WO_6 (E_{CB} = 0.515 eV, E_{VB} = 3.205 eV), which makes $BiVO_4$ to be a suitable material for constructing heterojunction with Bi_2WO_6. It's hoped that the $BiVO_4/Bi_2WO_6$ composite will exhibit good photocatalytic activity under visible light irradiation. Until now, few works have been concerned with $BiVO_4$ modification on visible-light photocatalyst Bi_2WO_6.

In this study, a series of $BiVO_4/Bi_2WO_6$ composites were synthesized by the combination of the homogeneous precipitation and hydrothermal methods and characterized by XRD, FTIR SEM, EDS, DRS, and PL techniques. The visible light photocatalytic activities of $BiVO_4/Bi_2WO_6$ for degradation of MB were greatly

improved as compared to either pure $BiVO_4$ or Bi_2WO_6. The mechanism of enhanced photocatalytic activity based on the band structures of $BiVO_4$ and Bi_2WO_6 was also discussed.

2. Experimental

2.1. Preparation of photocatalysts

The pure $BiVO_4$ was prepared by EDTA assisted coprecipitation method. In a typical synthesis, 10 mmol $Bi(NO_3)_3\ 5H_2O$ was dissolved in 2 M nitric acid to obtain solution A. Meanwhile, 10 mmol of NH_4VO_3 was dissolved in 2 M NaOH solution, and then 2 g of EDTA was added into the solution to form solution B. The resulting solution B was added drop-wise into solution A under ultrasound and the pH of the final suspension was adjusted to 7 by using NaOH solution. After reacting for some time, the as-formed precipitates were filtration, washed, dried and finally calcined at 500℃ for 3 h.

The $BiVO_4/Bi_2WO_6$ composites were prepared by the combination of the homogeneous precipitation and hydrothermal process. In a typical synthesis, 5 mmol $Bi(NO_3)_3\ 5H_2O$ and 2.5 mmol $Na_2WO_4\ 2H_2O$ were first dissolved in 2 M HNO_3 solution and deionized water, respectively, and these two solutions were mixed together to get a stable mixture. Then, certain amounts of $BiVO_4$ powders were added to the prepared mixture solution to form suspensions with different $BiVO_4$:Bi_2WO_6

mole ratios. The pH of the suspension was then adjusted to 7 by NaOH solution. After reacting for 1 h under ultrasound, the suspension was transferred into a Teflon-lined stainless steel autoclave and the hydrothermal reaction was carried out at 180℃ for 10 h. Then, the precipitates were filtered, washed and dried. Besides, the pure Bi_2WO_6 were also prepared for comparison by the same method.

2.2. Characterization of photocatalysts

The micro-structure and crystallinity of the photocatalysts were investigated by a D-MAX 2500/PC (Rigaku, Japan) X-ray diffractometer with the 2θ ranging from 10° to 70°. The morphology of the samples was examined by JSM-6700F Cold Field Emission Scanning Electron Microscope (JEOL, Japan). The energy-dispersive spectroscopy (EDS) was also performed during the SEM measurement. The Fourier transform infrared spectra (FT-IR) of the samples were obtained through a Nicolet 510P FT-IR spectrometer (Nicolet, America), using KBr as diluents. UV–Vis diffuse reflection spectroscopy (DRS) was determined with a UV-Vis-NIR spectrophotometer (Cary 500, America) in the range of 350-800 nm using $BaSO_4$ as the reference. The photoluminescence (PL) spectra, was recorded on a F-7000 fluorescence spectrophotometer (Hitachi, Japan) at room temperature with an excitation wavelength of 370 nm.

2.3. Photocatalytic activity tests

The photocatalytic activity of the samples was evaluated by the degradation of MB under visible light irradiation. A 300 W iodine-wolfram lamp was used as the light source, and a cut-filter was placed between the lamp and the reaction solution to remove the light with wavelengths less than 400 nm. In each experiment, 0.1 g photocatalyst was added into 100 mL MB solution (10 mg L^{-1}). Prior to illumination, the suspension was magnetically stirred in darkness for 30 min to ensure an adsorption/desorption equilibrium for MB solution and photocatalyst. At an irradiation interval of every 30 min, 5 mL suspensions were collected and centrifuged to remove the photocatalyst particles. Then the absorbance of MB was monitored with a UV–Vis spectrophotometer (UV 5100 B) at 664 nm during the photodegradation process.

3. Results and discussion

3.1. XRD analysis

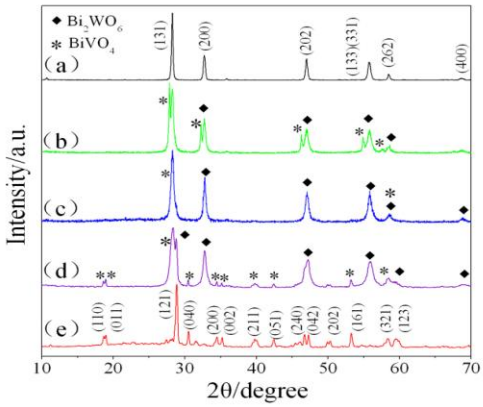

Fig.1. XRD patterns of different samples: (a) Bi_2WO_6, (b) $0.1BiVO_4$:$0.9Bi_2WO_6$, (c) $0.3BiVO_4$:$0.7Bi_2WO_6$, (d) $0.5BiVO_4$:$0.5Bi_2WO_6$, (e) $BiVO_4$

Fig. 1 presents the XRD patterns of the as-prepared photocatalysts with different $BiVO_4$ contents. Fig. 1a shows that the peaks of pure Bi_2WO_6 were readily indexed to the orthorhombic phase of Bi_2WO_6 (JCPDS No.39-0256). As revealed in Fig. 1e, the diffraction peaks of pure $BiVO_4$ agreed well with those of the monoclinic $BiVO_4$ (JCPDS card No. 14-0688). As for $BiVO_4$/Bi_2WO_6 composites (Fig. 1b, 1c and 1d), it can be seen that all of them exhibited a coexistence of both monoclinic $BiVO_4$ and orthorhombic Bi_2WO_6 phases, indicating that Bi_2WO_6 and $BiVO_4$ doped together successfully. The calcined $BiVO_4$ sample was less crystallized, resulting in more defects in the crystal, which were beneficial to the separation of the photo-generated electron-hole pairs in a sense[25].

3.2. FT-IR analysis

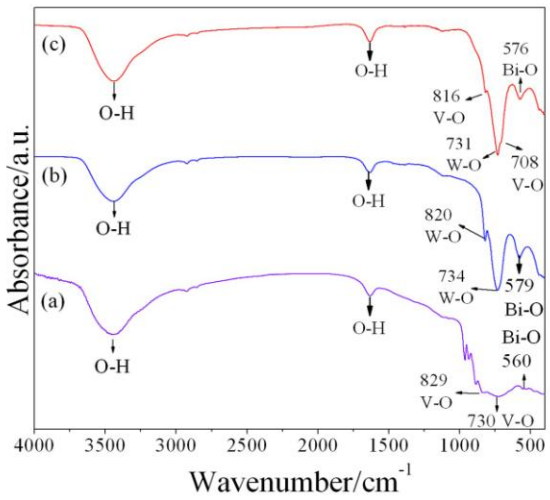

Fig.2. FT-IR spectra of (a) $BiVO_4$, (b) Bi_2WO_6, and (c) $0.3BiVO_4$:$0.7Bi_2WO_6$

FT-IR spectra of $BiVO_4$, Bi_2WO_6, and $0.3BiVO_4$:$0.7Bi_2WO_6$ are shown in Fig.2. The broad absorptions at 3445 cm^{-1} and 1629 cm^{-1} were related to H–O–H band of the

adsorbed water molecules. Fig. 2a shows an intense and broad band that included the characteristic bands of $BiVO_4$ oxide. The symmetric and asymmetric stretching vibrations of V-O at 730 cm^{-1} and 829 cm^{-1}, and the bending vibration band of Bi-O at 560 cm^{-1}[26].The characteristic bands of Bi_2WO_6 (Fig. 2b) assigned to the symmetric and asymmetric stretching vibration of W–O (820 cm^{-1},734 cm^{-1}) and the stretching vibration of Bi–O (579 cm^{-1}) were found.

For the $0.3BiVO_4$:$0.7Bi_2WO_6$ composite (Fig.2c), the symmetric and asymmetric stretching vibrations of V–O shifted to 708 cm^{-1} and 816 cm^{-1} while the peak existing at 731 cm^{-1} could be attributed to stretching vibrations of W–O. Besides, the bending vibration band of Bi–O at 576 cm^{-1} was also observed. As compared to the peaks of functional groups of $BiVO_4$ and Bi_2WO_6, the $0.3BiVO_4$:$0.7Bi_2WO_6$ had a similar spectrum, which indicated the $BiVO_4$ was successfully doped into Bi_2WO_6 in the hydrothermal reaction.

3.3. SEM and EDS observations

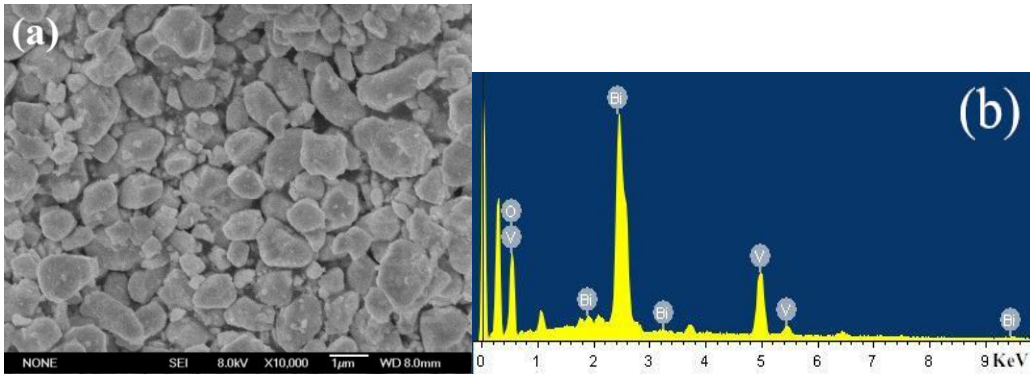

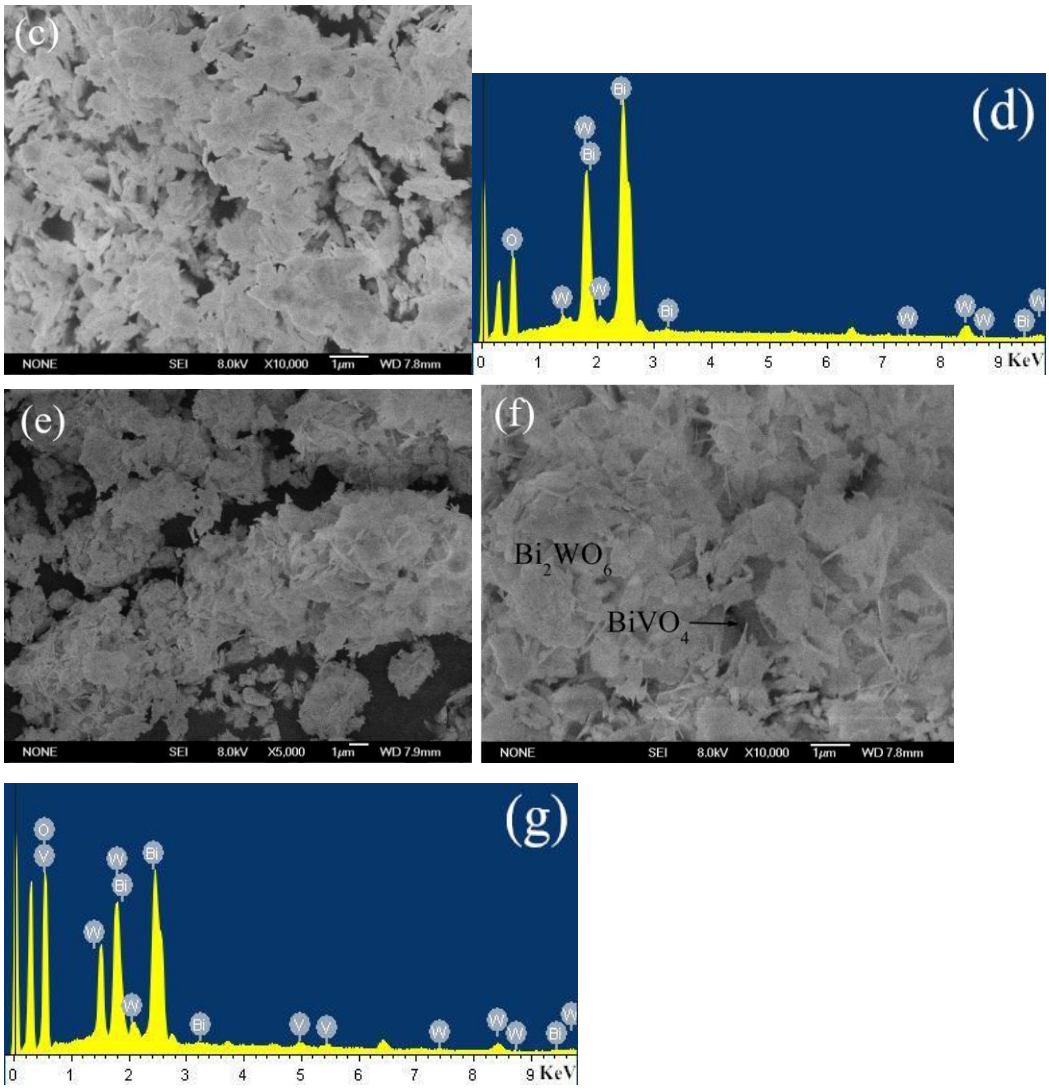

Fig. 3 SEM images and corresponding EDS patterns of $BiVO_4$ (a and b), Bi_2WO_6 (c and d), $0.3BiVO_4$:$0.7Bi_2WO_6$ (e, f and g)

The SEM and EDS photographs of the samples are presented in Fig. 3. As shown in Fig. 3a, $BiVO_4$ was consisted of irregular blocky structures with the size ranging from 0.2 μm to 1.8 μm. the surfaces and edges of the mono-dispersed lump are not smooth, which was advantageous to form the heterojunctions between Bi_2WO_6 and $BiVO_4$. Bi_2WO_6 nanoplates with rod-shaped structures could be clearly observed in Fig. 3b. It could be speculated that these nanoplates with uneven edges may be

formed by the bar agglomeration during hydrothermal process.

Low-magnification image of $BiVO_4/Bi_2WO_6$ compounds in Fig. 3e exhibited some flower-like aggregations. High magnification SEM image in Fig. 3f further revealed that these aggregations were formed by Bi_2WO_6 growth on the surface of $BiVO_4$. More importantly, Bi_2WO_6 scattered itself evenly over the surfaces of $BiVO_4$ blocks and developed close interactions with $BiVO_4$ which would further facilitate the formation of heterojunctions.

From Fig. 3b and 3d, one can see that the as-synthesized $BiVO_4$ and Bi_2WO_6 were consisted of Bi, V, O and Bi, W, O elements, respectively. EDS spectrum (Fig. 3g) was also performed to determine the Bi, W, V and O as major elements for $BiVO_4/Bi_2WO_6$ compounds.

3.4. UV-Vis DRS

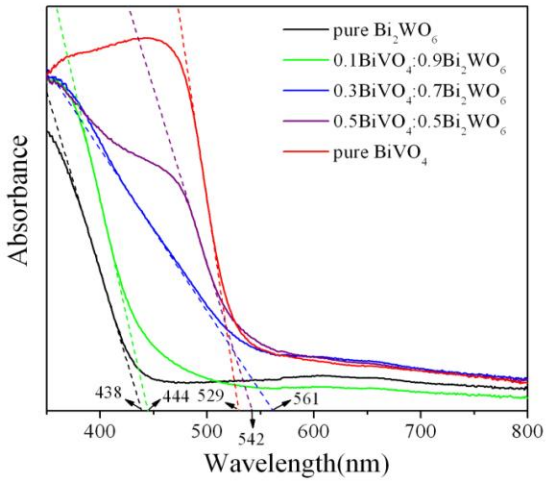

Fig.4. UV-Vis diffuse reflectance spectra of the as-synthesized samples.

Fig. 4 displays the diffuse reflectance spectra of $BiVO_4/Bi_2WO_6$ composite

photocatalysts with different $BiVO_4$ contents. It can be noted that with the increasing of $BiVO_4$ content, the absorption intensity of composites increased with varying degrees as compared to pure Bi_2WO_6 in the region of 350-550 nm and the absorption edge had a significantly red shift. Additionally, the steep shape of the spectrum indicated that the visible light absorption was not due to the transition from the impurity level but was due to the band gap transition[27].

The absorption onsets of the samples were measured by linear extrapolation from the inflection point of the curve to the baseline, reaching a quantitative estimate of the band gap energies[28]. The band gap energy values (Eg, eV) for different samples were calculated using the equation[29]:

$$Eg\ (eV) = 1240/\lambda\ (nm) \quad (1)$$

Where λ represents the wavelength of the absorption onset. The Eg of Bi_2WO_6, $0.1BiVO_4$:$0.9Bi_2WO_6$, $0.3BiVO_4$:$0.7Bi_2WO_6$, $0.5BiVO_4$:$0.5Bi_2WO_6$ and $BiVO_4$ were 2.83, 2.79, 2.21, 2.29 and 2.34 eV, respectively. From the result, we can see that the $0.3BiVO_4$:$0.7Bi_2WO_6$ sample showed the minimum band gap energy value, which implied it had the highest photocatalytic activity. In other words, the modification of $BiVO_4$ tended to narrow the band gap of Bi_2WO_6 photocatalyst, which would result in improvement of visible light responses and higher photocatalytic activities.

3.5. Photocatalytic degradation of MB under visible light irradiation

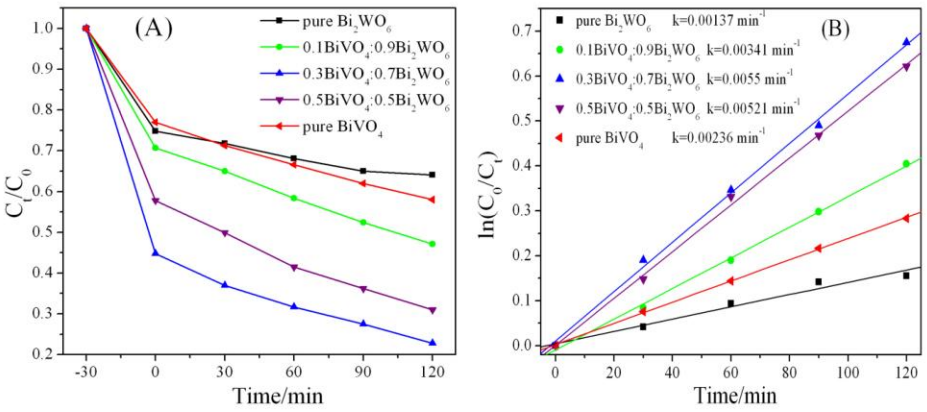

Fig.5. Photocatalytic degradation efficiency of MB by different photocatalysts under visible light (A) and the dynamic of MB degradation reaction (B)

Photocatalytic performance of as-fabricated catalysts was evaluated by decomposition of MB under visible light irradiation. Fig. 5A shows the efficiencies of the photocatalytic degradation, where C_t was the concentration of MB during the reaction and C_0 was the initial concentration of MB solution (before adsorption equilibrium on $BiVO_4/Bi_2WO_6$ composites), respectively. As depicted in Fig. 5A, the removal rates of MB concentration in the presence of pure Bi_2WO_6 or pure $BiVO_4$ were only about 35.9% and 42.0% after 120 min under visible light irradiation. As for $BiVO_4/Bi_2WO_6$ composites, obvious enhancement of degradation efficiency was found. Obviously, the highest photocatalytic activity was achieved when the mole ratio of $BiVO_4$ and Bi_2WO_6 was 0.3:0.7. The adsorption quantity of Bi_2WO_6, $0.1BiVO_4$:$0.9Bi_2WO_6$, $0.3BiVO_4$:$0.7Bi_2WO_6$, $0.5BiVO_4$:$0.5Bi_2WO_6$ and $BiVO_4$ after magnetically stirred in darkness for 30 min reaches 25.2%, 29.3%, 55.2%, 42.2% and 23.0%, respectively. The adsorbability of $0.3BiVO_4$:$0.7Bi_2WO_6$ catalyst was also the

best among all the samples, which proved that better adsorbability was also favorable for excellent photocatalytic performance.

It is well known that when the pollutant is within the millimolar concentration range, photocatalytic oxidation of organic pollutants follows first-order kinetics[30], as shown by Eq. (2):

$$\ln (C_0/C_t) = kt + a \quad (2)$$

Where C_0 and C_t are the dye concentrations in solution at times 0 and t, respectively, and k is the apparent first-order rate constant. In Fig. 5B, it can be seen that the k was maximum when the $BiVO_4$ content was 0.3 (mole ratio), showing that the reaction rate of $0.3BiVO_4$:$0.7Bi_2WO_6$ sample was the highest. Furthermore, the k for MB photodegradation over $0.3BiVO_4$:$0.7Bi_2WO_6$ catalyst was about 4.0 and 2.3 times higher than that of pure Bi_2WO_6 and pure $BiVO_4$, respectively.

3.6. Photocatalytic mechanism

To further investigate the effect of the $BiVO_4$ modification, the PL spectra of $BiVO_4$/Bi_2WO_6 (Fig. 6) with 370 nm excitation wavelength was carried out. PL spectra was commonly employed to study the immigration, transfer, and charge carrier trapping processes and to investigate the fate of e^-/h^+ pairs in semiconductor particles[31].The lower PL intensity usually indicates the higher separation efficiency of photoinduced charge, thus the higher photocatalytic activity[32].

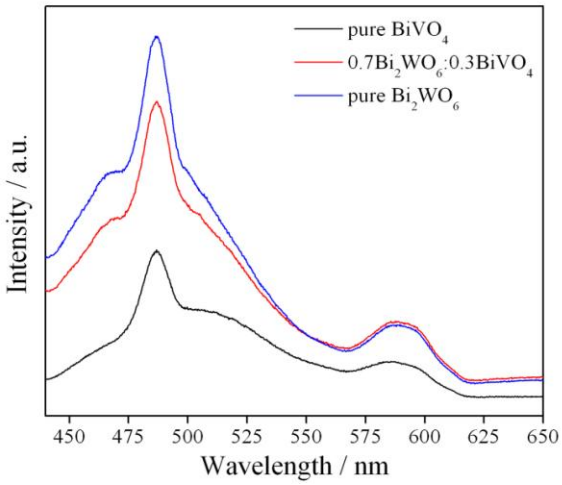

Fig.6. PL spectra of pure $BiVO_4$, $0.3BiVO_4$:$0.7Bi_2WO_6$ and pure Bi_2WO_6 photocatalysts recorded at room temperature with the excitation wavelength of 370 nm.

From Fig. 6, it was found that the tested three catalysts showed the main peaks at similar position but with different intensities: a strong sharp peak at 487 nm and a broad weak peak at 587 nm. $BiVO_4$/Bi_2WO_6 composite showed diminished intensity in comparison to pure Bi_2WO_6 before 550 nm, indicating that the introduction of $BiVO_4$ would improve the separation efficiency of the carriers generated in Bi_2WO_6. Interestingly, the PL peak of pure $BiVO_4$ was lower than that of the $BiVO_4$/Bi_2WO_6 composite though $BiVO_4$ exhibited much lower photocatalytic activity under visible light, which was similar to the results of the reported documents[33]. Further researches are still being carried out to reveal relevant mechanisms.

As we all know, the process of photocatalysis was pr opelled by the absorption of photon of the band gap to excite electrons from valence band to conduction band, and subsequently, separated electrons and holes moved to composite surface and react.

Thus, the narrower band gap is, the more activity the photocatalyst has. After decorated by $BiVO_4$, the forbidden band of Bi_2WO_6 whose width was 2.83 eV dropped to 2.21 eV, the light absorption was enhanced and the recombination of electron-hole pairs was reduced. Based on the existing results, we can conclude that the enhancement of photocatalytic activity of $BiVO_4/Bi_2WO_6$ composite photocatalysts was due to the improvement of light absorption, the better adsorbability, the decrease of band gap energy and the lower recombination efficiency of e^-/h^+ pairs.

On the basis of reported researches[34][35] and our experiment results, we have proposed a possible photodegradation mechanism of the $BiVO_4/Bi_2WO_6$ composites:

$$BiVO_4/Bi_2WO_6 + MB \longrightarrow BiVO_4/Bi_2WO_6\text{-}MB \quad (3)$$

$$BiVO_4 + h\nu \longrightarrow BiVO_4\,(h^+ + e^-) \qquad Bi_2WO_6 + h\nu \longrightarrow Bi_2WO_6\,(h^+ + e^-) \quad (4)$$

$$BiVO_4\,(e^-) + Bi_2WO_6 \longrightarrow Bi_2WO_6\,(e^-) + BiVO_4$$

$$Bi_2WO_6\,(h^+) + BiVO_4 \longrightarrow BiVO_4\,(h^+) + Bi_2WO_6 \quad (5)$$

$$Bi_2WO_6\,(e^-) + O_2 \longrightarrow Bi_2WO_6 + O_2^{\cdot-} \qquad H^+ + O_2^{\cdot-} \longrightarrow \cdot OH$$

$$BiVO_4\,(h^+) + OH^- \longrightarrow BiVO_4 + {}^{\cdot}OH \quad (6)$$

$${}^{\cdot}OH + MB \longrightarrow \text{degraded product} \quad (7)$$

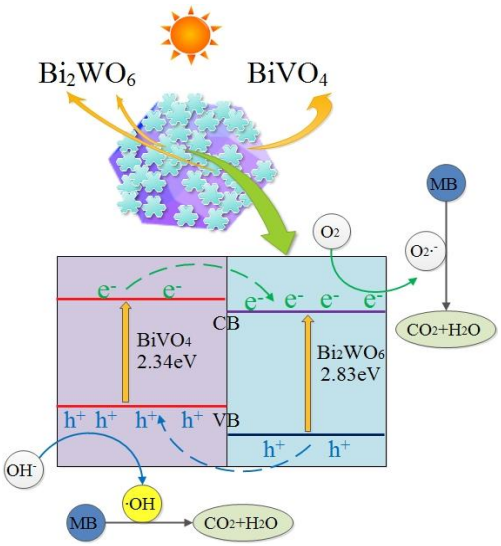

Fig.7. Mechanism of photodegradation over $BiVO_4/Bi_2WO_6$ composite photocatalyst under visible light irradiation

The possible photo-catalytic mechanism can be schematically described in Fig.7. The photogenerated electrons in Bi_2WO_6 were captured by O_2 to yield $O_2^{\cdot-}$ and the holes in $BiVO_4$ are trapped by OH^- to produce $\cdot OH$. $O_2^{\cdot-}$ and $\cdot OH$ play an important role in the photodegradation process, and would further oxidize the MB molecules to form CO_2 and H_2O completely.

4. Conclusions

Visible-light-driven $BiVO_4/Bi_2WO_6$ photocatalysts with different mole ratios have been successfully prepared by a hydrothermal method. XRD patterns revealed that the as-prepared composites were composed of monoclinic $BiVO_4$ and orthorhombic Bi_2WO_6. The addition of $BiVO_4$ significantly improved the photocatalytic activity of Bi_2WO_6 under visible light irradiation. The optimized

catalyst with a mole ratio of 0.3:0.7 ($BiVO_4$:Bi_2WO_6) had the highest activity. It can be concluded that the enhancement of photocatalytic performance of $BiVO_4$/Bi_2WO_6 composite photocatalysts was because of the improvement of light absorption, the excellent adsorbability, the narrow band gap and high separation efficiency of photo-induced charges.

Reference

[1] W.K. Ho, J.C. Yu and S.C. Lee, *J. Solid State Chem.*, 2006, **179**, 1171-1176.

[2] C.L. Yu, J.C. Yu and M. Chan, *J. Solid State Chem.*, 2009, **182**, 1061–1069.

[3] M. Shang, W.Z. Wang, S.M. Sun, L. Zhou and L. Zhang, *J. Phys. Chem. C*, 2008, **112**, 10407–10411.

[4] Y.L.Kuo, H.W. Chen and Y. Ku, *Thin Solid Films*, 2007, **515**, 3461–3468.

[5] Z. Ambrus, N. Balazs, T. Alapi, G. Wittmann, P. Sipos, A. Dombi and K. Mogyorosi, *Appl. Catal. B: Environ.*, 2008, **81**, 27–37.

[6] S.W. Yang and L. Gao, *J. Am. Ceram. Soc.*, 2004, **87**, 1803-1805.

[7] A. Naldoni, M. D'Arienzo, M. Altomare, M. Marelli, R. Scotti, F. Morazzoni, E.Selli and V.D. Santo, *Appl. Catal. B: Environ.*, 2013, **130–131**, 239–248.

[8] K.E. deKrafft, C. Wang and W.B. Lin, *Adv. Mater.*, 2012, **24**, 2014–2018.

[9] J.W. Tang, Z.G. Zou and J.H. Ye, *Chem. Mater.*, 2004, **16**, 1644-1649.

[10] Z. Zou, J. Ye, K. Sayama and H. Arakawa, *Chem. Phys. Lett.*, 2001, **333**, 57-62.

[11] X.K. Wang, G.C. Li, J. Ding, H.R. Peng and K.Z. Chen, *Mater. Res. Bull.*, 2012, **47**, 3814–3818

[12] C.C. Mao, M.L. Li, Z.G. Fang, F.l. Meng, X.N. Qu, Y.P. Liu, M.J. Wang, J. Zhang, Z. Shi and X.H. Guo, *RSC Adv.*, 2012, **2**, 5513–5515.

[13] S.Xie, K. OuYang and X.O. Ma, *Ceram. Int.*, 2014, **40**, 12353–12357.

[14] S.L. Wang, L.L. Wang, W.H. Ma, D.M. Johnson, Y.F. Fang, M.K. Jia, Y.P. Huang, *Chem. Eng. J.*, 2015, **259**, 410–416.

[15] C. Zhang and Y.F. Zhu, *Chem. Mater.*, 2005, **17**, 3537-3545.

[16] Y. Huang, Z.H. Ai, W.K. Ho, M.J. Chen and S.C. Lee, *J. Phys. Chem. C*, 2010, **114**, 6342–6349.

[17] Z.J. Zhang, W.Z. Wang, M. Shang and W.Z. Yin, *J. Hazard. Mater.*, 2010, **177**, 1013–1018.

[18] L. Wu, J.L. Bi, Z.H. Li, X.X. Wang and X.Z. Fu, *Catal. Today*, 2008, **131**, 15–20.

[19] Q.C, Xu, D.V. Wellia, Y.H. Ng, R. Amal and T.T.Y. Tan, *J. Phys. Chem. C*, 2011, **115**, 7419–7428.

[20] S. Guo, X.F. Li, H.Q. Wang, F. Dong and Z.B. Wu, *J. Colloid Interface Sci.*, 2012, **369**, 373–380.

[21] H.W. Huang, S.B. Wang, N. Tian and Y.H. Zhang, *RSC Adv.*,2014, **4**, 5561 –5567.

[22] X.L. Liu, M.J. Zhou, G.X. Yao, W.D. Shi, C.C. Ma, P. Lv, Y.F. Tang and Y.S. Yan, *RSC Adv.*, 2014, **4**, 18264–18269.

[23] S.M. Sun, W.Z. Wang, L. Zhang and J.H. Xu, *Appl. Catal. B*, 2012, **125**, 144–148.

[24] S. Kohtani, M. Koshiko, A. Kudo, K. Tokumura, Y. Ishigaki, A. Toriba, K. Hayakawa and R. Nakagaki, *Appl. Catal. B: Environ.*, 2003, **46**, 573-586.

[25] Z.C. Kang and Z.L. Wang, *J. Phys. Chem.*, 1996, **100**, 5163–5165.

[26] U.M.G. Perez, S. Sepulveda-Guzman, A. Martinez-de la Cruz and U.O. Mendez, *J. Mol. Catal. A: Chem.*, 2011, **335**, 169–175.

[27] A. Kudo, I. Tsuji and H. Kato, *Chem. Commun.*, 2002, **17**, 1958–1959.

[28] M. Wang, H.Y. Zheng, Q. Liu, C. Niu, Y.S. Che and M.Y. Dang, *Spectrochim. Acta, Part A*, 2013, **114**, 74–79.

[29] L. Ge and L.S. Cui, *J. Chin. Ceram. Soc.*, 2008, **36**, 320–324.

[30] L. Ge, C.C. Han and J. Liu, *Appl. Catal. B*, 2011, **108–109**, 100–107.

[31] G. Eda, Y.Y. Lin. C. Mattevi, H. Yamaguchi, H.A. Chen, I.S. Chen, C.W. Chen and M. Chhowalla, *Adv. Mater.*, 2010, **22**, 505-509.

[32] H. Xu, H.M. Li, C.D. Wu, J.Y. Chu, Y.S. Yan and H.M. Shu, *Mater. Sci. Eng. B*, 2008, **147**, 52–56.

[33] S.Y. Wu, H. Zheng, Y.W. Lian and Y.Y. Wu, *Mater. Res. Bull.*, 2013, **48**, 2901–2907.

[34] Z.J. Zhang, W.Z. Wang, L. Wang and S.M. Sun, *ACS Appl. Mater. Interfaces*, 2012, **4**, 593–597.

[35] J. Su, X.X. Zou, G.D. Li, X. Wei, C. Yan, Y.N. Wang, J. Zhao, L.J. Zhou and J.S. Chen, *J. Phys. Chem. C*, 2011, **115**, 8064-8071.